Nanoscale

RSC Publishing

PAPER

Native amorphous nanoheterogeneity in gallium germanosilicates as a tool for driving Ga_2O_3 nanocrystal formation in glass for optical devices

Cite this: *Nanoscale*, 2013, 5, 299

Vladimir N. Sigaev,[a] Nikita V. Golubev,[a] Elena S. Ignat'eva,[a] Bernard Champagnon,[b] Dominique Vouagner,[b] Eric Nardou,[b] Roberto Lorenzi[c] and Alberto Paleari*[ac]

Nanoparticles in amorphous oxides are a powerful tool for embedding a wide range of functions in optical glasses, which are still the best solutions in several applications in the ever growing field of photonics. However, the control of the nanoparticle size inside the host material is often a challenging task, even more challenging when detrimental effects on light transmittance have to be avoided. Here we show how the process of phase separation and subsequent nanocrystallization of a Ga-oxide phase can be controlled in germanosilicates – prototypal systems in optical telecommunications – starting from a Ga-modified glass composition designed to favour uniform liquid–liquid phase separation in the melt. Small angle neutron scattering data demonstrate that nanosized structuring occurs in the amorphous as-quenched glass and gives rise to initially smaller nanoparticles, by heating, as in a secondary phase separation. By further heating, the nanophase evolves with an increase of nanoparticle gyration radius, from a few nm to a saturation value of about 10 nm, through an initial growing process followed by an Ostwald ripening mechanism. Nanoparticles finally crystallize, as indicated by transmission electron microscopy and X-ray diffraction, as γ-Ga_2O_3 – a metastable gallium oxide polymorph. Infrared reflectance and photoluminescence, together with the optical absorption of Ni ions used as a probe, give an indication of the underlying interrelated processes of the structural change in the glass and in the segregated phase. As a result, our data give for the first time a rationale for designing Ga-modified germanosilicates at the nanoscale, with the perspective of a detailed nanostructuring control.

Received 17th September 2012
Accepted 25th October 2012

DOI: 10.1039/c2nr32790b

www.rsc.org/nanoscale

Introduction

Nucleation and crystallization processes in glasses are topical arguments both in view of the fundamental interest in the physical and chemical mechanisms involved – including liquid–liquid phase transformations in the melt as one of the possible origins of glass heterogeneities acting as nucleating sites[1] – and for the large number of technological applications one can potentially design from nanostructure-based functionalisation strategies.[2] In particular, as concerns technology, controlled glass devitrification at the nanoscale is crucially connected with the fabrication of nanocrystalline glassceramic (GC) fibres. In fibres, embedded nanocrystals can act as a suitable host for optically active ions.[3] In this regard, silicate GCs have recently attracted much attention as optical light-emitting systems, either exploiting nanocrystal intrinsic luminescence or radiative transitions of optical active ions.[4–7] From this point of view, gallium oxide nanoparticles in glass appear interesting as a suitable host for transition metal ions, mainly Ni^{2+} and Cr^{4+}, in view of obtaining efficient broadband near-infrared emission.[8–16] As a matter of fact, transition metal ions often exhibit only weak or even no luminescence in amorphous hosts, because of strong nonradiative relaxation mechanisms. Nevertheless, the ordered environment offered by nanocrystals to optically active ions can instead minimize the fluorescence quenching and provide large cross-sections for absorption and stimulated emission. Promising luminescence properties have recently been observed both in silicate GCs and germanosilicate GCs, after nanocrystallization of gallium-containing spinel nanocrystals and also forsterite nanocrystals.[10,17–24] Importantly, the possibility of obtaining optical quality GC materials mainly depends on two factors: first, on the size of nanocrystals, which have to be much smaller (usually less than 10–50 nm) than the wavelength of the visible light and second, on the refractive index values of the two phases (nanocrystals and glass), which should not be too different.[25] Therefore, the control of the

[a]*International Laboratory of Glass-based Functional Materials, Mendeleev University of Chemical Technology of Russia, Miusskaya Square 9, 125190 Moscow, Russia*
[b]*Université de Lyon, Université Lyon 1, UMR5620 CNRS, Laboratoire de Physico-Chimie des Matériaux Luminescents, Domaine scientifique de la Doua, Bât. Kastler, 10 rue Ampère, Villeurbanne, F-69622, France*
[c]*Department of Materials Science, University of Milano-Bicocca, Via R. Cozzi 53, I-20125 Milano, Italy. E-mail: alberto.paleari@unimib.it; Fax: +39 02 64485400; Tel: +39 02 64485164*

nanocrystal size or, more generally, of the extent of the phase separation – which determines the density and refractive index contrast between the nanophase and the matrix – is crucial to optimize this kind of systems and also to understand the underlying processes of nanocrystallization. In the specific case of Ga-containing germanosilicate GCs, there is evidence of variations of the crystalline domain size at a fixed size of Ga-oxide nanoparticles as a function of Ni-doping.[24] This apparently suggests that Ni has a role as a crystallizing agent. However, since crystallization also occurs without Ni-doping, Ni ions cannot be identified as main nucleating sites in the phase separation. As a matter of fact, lacking any detailed indication about the glass configuration from which nanocrystallization can start, empirical strategies have only been used up to now to optimize these systems.

In the present work, aimed at achieving a more defined understanding of the Ga-induced nanostructuring process in glass, we have investigated the evolution of the nano-inhomogeneous structure in alkali gallium germanosilicate glass between T_g and the maximum of the exothermic peak of nanophase crystallization. The nanoinhomogeneous glass configuration has been investigated in its amorphous state – before crystallization – taking advantage of the potential of small-angle neutron scattering (SANS) in giving information on the elusive features of glass nanostructuring processes.[26] Formation and evolution of the crystal nanophase have been analyzed by high-resolution transmission electron microscopy (TEM) and X-ray diffraction (XRD). Finally, some insights into the coordination structure of the separated phases have been obtained by means of Fourier-transform infrared (FT-IR) reflectance spectroscopy, optical absorption data, and photoluminescence spectra. The results give clear-cut evidence of glass–glass nanostructuring – similar to what has very recently been demonstrated in aluminosilicates,[27] but starting from a native phase separation on a larger scale in the still amorphous glass – with successive growth of a separated Ga-oxide phase with a strong readjustment of the coordination structure mediated by non-bridging oxygen. Importantly, the process limits the nanoparticle size at about 20 nm, even after prolonged thermal treatment at the crystallization temperature. The data give for the first time a clear perspective for the optimization of this system for applications, offering a rationale for nanostructuring control.

Materials and procedure

Glass with nominal composition $7.5Li_2O$–$2.5Na_2O$–$20Ga_2O_3$–$35SiO_2$–$35GeO_2$ doped with 0.1 NiO (mol%) was prepared by a conventional melt-quenching method. The raw materials are amorphous SiO_2 (special purity grade), GeO_2 (special purity), Li_2CO_3 (reagent grade), Na_2CO_3 (reagent grade), Ga_2O_3 (reagent grade) and NiO (reagent grade). The amount of reagent in each batch was calculated in order to prepare 120 g of final product. The starting materials were weighed using an analytical balance with an accuracy of 0.001 g and carefully mixed in an agate mortar. Glasses were then prepared in a 40 ml crucible in air at 1480 °C for 40 min. As-quenched bulk samples were heat-treated at various temperatures in order to obtain transparent glass-ceramics. Heat treatment was performed in air by putting the glass samples into the muffle furnace with an accuracy on the heat treatment temperature of ±1 K.

Differential scanning calorimetry (DSC) measurements were performed by means of a Netzsch DSC 449F3 high-temperature thermoanalyzer in platinum crucibles, at a heating rate of 10 K min^{-1} in Ar, on bulk samples of 10–15 mg. X-ray diffraction patterns of the powdered samples were recorded on a DRON 3M diffractometer (CuK_α radiation, Ni filter). Particular attention has been paid to specimen preparation, mainly as regards powder granulometry and sample positioning, so as to minimize the error in the evaluation of the integrated signal used to estimate the crystallised volume fraction. Crystalline phases were identified by comparing relative intensities of peaks in X-ray diffraction patterns and their positions with the data available in the JCPDS (Joint Committee on Powder Diffraction Standards) database. Transmission electron microscopy (TEM) images and diffraction patterns were obtained using a field emission gun transmission electron microscope FEI Tecnai G2 F20, with an accelerating voltage of 200 kV and equipped with an S-Twin lens that gives a point resolution of 0.24 nm. The imaging system is composed of one tv rate 626 Gatan and one slow scan 794 Gatan CCD camera. Samples were prepared as a finely ground powder and deposited on a gold microscopy grid. No effect of electron irradiation on the nanostructured materials was observed during low resolution TEM measurements. Evidence of partial nanophase amorphisation and matrix degradation was detected only after prolonged exposure under high-resolution focusing conditions. Room temperature SANS curves were obtained on samples prepared as disks with a diameter of approximately 10 mm and a thickness of 2 mm. SANS measurements were performed both on samples previously heat treated at different temperatures or time durations and on glass samples heated in a high-temperature furnace in the SANS apparatus. The dependence of the SANS intensity I on the scattering vector $q = 4\pi\sin\theta/\lambda$ in the range $0.003\ Å^{-1} < q < 0.2\ Å^{-1}$ was measured on the *D11* diffractometer installed in a high-flux nuclear reactor at the Institute Laue-Langevin (Grenoble, France). The gyration radii and diameters of inhomogeneities were determined in the Guinier approximation, *i.e.* from the slope of the straight-line portion of the small-angle curve in $\ln(I)$–q^2 coordinates in the range of small scattering vectors q under the assumption that there is a statistically uniform distribution of spherical particles in the homogeneous matrix. The square of the difference between the inhomogeneity and matrix densities $\langle(\Delta\rho)^2\rangle = \rho^2 c(1 - c)$, where c is the volume fraction of one of the phases, was calculated by integrating the function $I(q)\cdot q^2$.

Spectroscopic measurements were performed on bulk samples, about 2 mm thick, both before and after different heat treatments, after surface polishing. Optical absorption spectra were collected in the spectral range from 300 to 1500 nm, with a spectral bandwidth of 1 nm, using a double-beam spectrophotometer Perkin Elmer Lambda 950. Micro-fluorescence analysis of the light-emitting activity caused by non-bridging oxygen sites was performed exciting at 633 nm by means of a He–Ne

laser in the back-scattering configuration and collecting the signal through a micro-Raman spectrometer Labram Jobin-Yvon with a spectral resolution of 0.3 nm. Infrared spectra were collected in the range 400–4000 cm^{-1} in reflection geometry with a micro-FTIR Nicolet iN10 under nitrogen flux, with a spectral resolution of 4 cm^{-1}.

Results and discussion

Nanostructuring control and design of specific nanostructures in glass have to start from the knowledge of at least two basic parameters – the glass transition temperature and the crystallization temperature. The absolute and relative positions of these processes on the temperature axis indeed determine much of the system propensity to give a nanostructured glass, since they fix glass stability, component diffusivity, and controllability of the crystallization process.[28] Then, it is necessary to get information on the phase, or phases, arising from the nanocrystallization. Finally, a picture of the detailed mechanisms underlying nanoparticle growth and crystallization is required.

This enables the design and optimization of the system according to the desired material functions – often related to nanoparticle size dispersion and concentration – by means of a correct choice of synthesis and/or treatment parameters. In the next sections, following just this rationale, we report thermodynamic and structural data on the nanophase, followed by the discussion of the possible involved mechanisms, based on the complementary information from SANS experiments and spectroscopic results.

Thermodynamics and nanocrystallisation

In Fig. 1 we report representative DSC curves of as-quenched bulk samples with the investigated composition, both with and without NiO doping at a concentration of 0.1 mol%. The curves register a change of slope below 600 °C, corresponding to the glass transition. Above 600 °C, glass crystallization begins to occur, up to the maximum rate of crystallization giving rise to a sharp exothermic peak at approximately 690 °C. Addition of 0.1 mol% NiO causes a decrease of less than 10 °C in the first exothermic peak. This shift confirms the role of Ni as a crystallizing agent, indicating however that the used doping does not cause drastic perturbation of the investigated glass system. The overall similarity between thermal evolution of samples with and without NiO addition confirms that the various steps of the phase separation process are largely determined by the other more abundant oxides in the composition.

The analysis of XRD patterns on samples treated at temperature close to the exothermic peak indeed confirms the formation of a crystalline phase. Fig. 2 reports the results on powered samples obtained from glass plates before and after heat treatment for different time durations. Three main facts are worth noting. First, the pattern of as-quenched glass, even though it is basically amorphous-like with the usual broad halo observed in glasses, shows an additional weak and broad shoulder at around $2\theta = 36°$, suggesting the occurrence of a sub-micrometer two-phase structure. No evidence of crystalline phases is detected at this stage.

Second fact – a set of reflections are detected as a result of heating at 690 °C, progressively narrower by prolonging treatment duration, at positions corresponding to diffraction peaks ascribable to both γ-Ga_2O_3 (JCPDS 20-0426) and $LiGa_5O_8$ (JCPDS

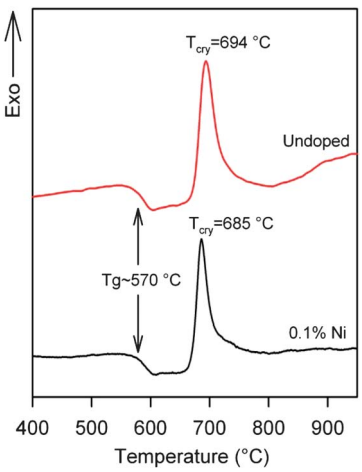

Fig. 1 DSC curves of as-quenched $7.5Li_2O$–$2.5Na_2O$–$20.0Ga_2O_3$–$35.0SiO_2$–$35.0GeO_2$ glass (mol%) without (red curve) and with 0.1% NiO doping (black curve).

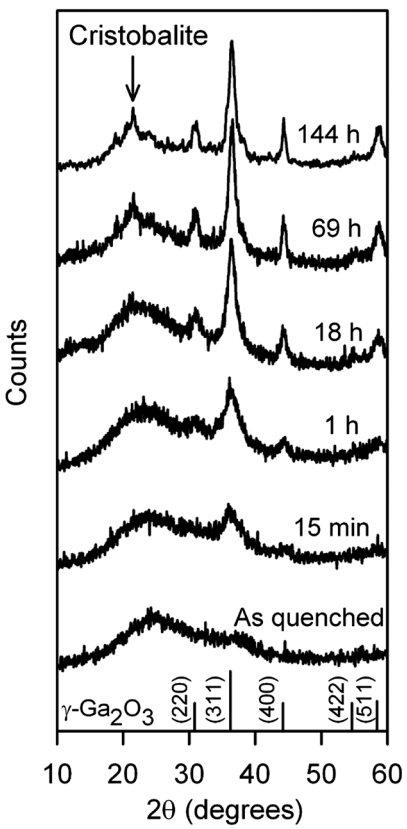

Fig. 2 XRD patterns of powdered samples of 0.1 NiO-doped $7.5Li_2O$–$2.5Na_2O$–$20.0Ga_2O_3$–$35.0SiO_2$–$35.0GeO_2$ glass treated at 690 °C for the indicated time. Positions and relative intensities of reflections of γ-Ga_2O_3 are reported for comparison, as well as the expected position of the main reflection from the SiO_2 cristobalite phase.

76-0199). To better identify the precipitated phase, we have considered the intensity ratio between the diffraction peaks at $2\theta = 36.2°$ and 44.1°. From literature data, this value is expected to be 8.1 and 5 for $LiGa_5O_8$ and γ-Ga_2O_3, respectively. In our case, this ratio is equal to 4.6 thus suggesting the precipitation of a spinel γ-Ga_2O_3 phase. The width of the (311) reflection at $2\theta = 36.19°$ (which falls just in the position of the shoulder observed in as-quenched glass) can be used to estimate the crystal domain diameter through Scherrer's formula $d = 0.9\lambda/(\Delta\cos\theta)$, where d is the average crystallite diameter, λ the X-ray wavelength, Δ the full width at half maximum in radians of the strongest diffraction peak. We obtain an estimated value of about 4 and 7 nm after treatment at 690 °C for 15 and 18 h, respectively. The volume fraction occupied by the crystalline nanophase has been estimated by evaluating the reduction of the total area of the broad glassy halo, before and after heat treatments, in measurements taken under similar experimental conditions. Importantly, the nanophase volume fraction indicates that it reaches values of about 15% and 21% after 18 and 69 h, respectively. Within the uncertainty of this kind of calculation, these values are consistent with the maximum expected value in the case of full crystallization, that is 24 vol% for the investigated nominal concentration of gallium oxide (20 mol%). However, this result does not exclude that a minor fraction of Ga oxide remains in the glass.

Third relevant outcome from XRD analysis is the good stability of both the crystallized nanophase and the glass matrix.

In fact, some preliminary form of matrix crystallization appears only after treatment prolonged for more than 18 h, with the formation of a small amount of cristobalite. In summary, as regards XRD data, the modifications in the X-ray diffraction patterns suggest that there is a pre-existent separated phase which undergoes progressive ordering and a moderate growth during heat treatments. As a matter of fact, the segregation of the crystalline phase, even when approaching the full nominal fraction of Ga oxide, keeps nanometer size. The formation of a gallium oxide spinel phase as a result of the structural ordering suggests that during thermal treatment the density difference between the initial inhomogeneities and the matrix increases through progressively Ga-enrichment of nanoparticles up to full crystallization.

Additional complementary support to this view comes from transmission electron microscopy. In Fig. 3 we report representative results of the analysis of TEM data on as-quenched (Fig. 3a, d and g) and heat treated samples at 690 °C for 2.5 h (Fig. 3b, e and h) and 90 h (Fig. 3c, f and i). Consistent with XRD data, the electron diffraction patterns of heat treated samples show clear diffraction features (Fig. 3h and i) ascribable to the crystalline γ-Ga_2O_3 phase (Fig. 3k). Moreover, as evidenced in images both at high (Fig. 3b and c) and low resolutions (Fig. 3e and f), the size of the nanoparticles is not much dependent on how long the treatment is, at least after the first hour of heating. In fact, the nanocrystal size turns out to be of the order of a few nm (Fig. 3j), analogous to the values estimated from XRD. As regards the analysis of as-quenched glass, the high-resolution

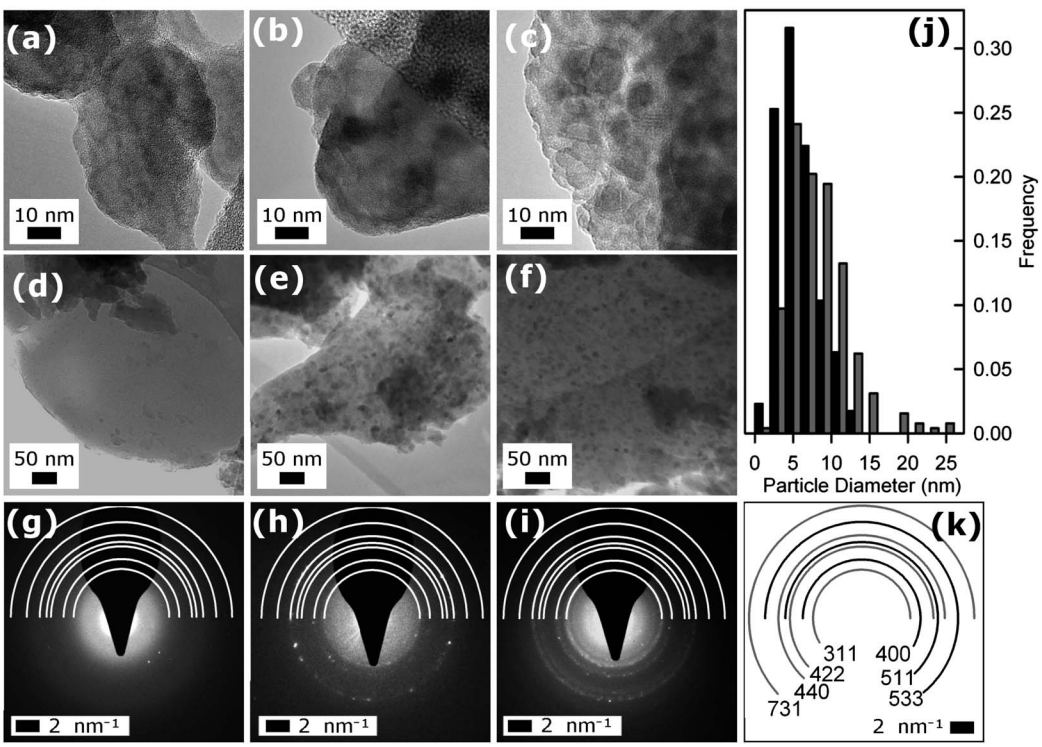

Fig. 3 TEM analysis of 0.1 NiO-doped $7.5Li_2O$–$2.5Na_2O$–$20.0Ga_2O_3$–$35.0SiO_2$–$35.0GeO_2$ heat-treated at 690 °C for different time durations. High resolution images of as-quenched (a), and heat treated samples at 690 °C for 2.5 h (b) and 90 h (c), with low-resolution images (d–f, respectively) and electron diffraction patterns (g–i, respectively). (j) Nanocrystal size statistics in treated samples (from e and f). (k) Labeled scheme of the diffraction pattern of γ-Ga_2O_3.

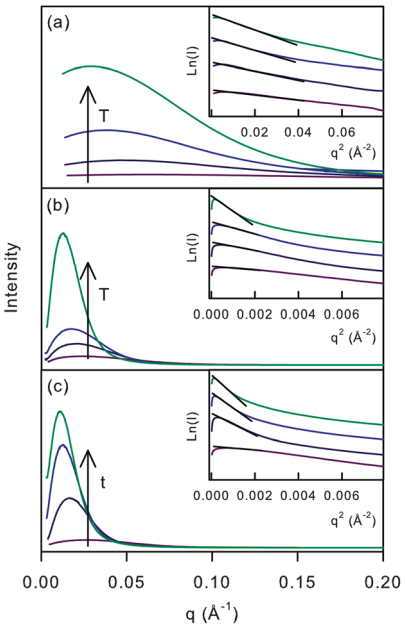

Fig. 4 SANS results – displayed as scattered intensity *vs.* wavevector q and (in insets) as Guinier plots of ln(I) *vs.* q^2 – on 0.1 NiO-doped $7.5Li_2O$–$2.5Na_2O$–$20.0Ga_2O_3$–$35.0SiO_2$–$35.0GeO_2$ samples at different steps of the nanostructuring process (straight lines in insets are guides to the eyes). (a) Data on a sample treated at successive 1 h heating in 10 °C steps after starting the pre-treatment of 70 min at 550 °C (curves after treatments at 590, 610, 620 and 630 °C are reported); (b) data collected from isochronal annealing experiments on samples treated for 18 h at 610, 630, 650, and 670 °C; (c) data of isothermal experiments on samples treated at 670 °C for different time durations t (curves at 0, 5, 18, and 40 h are reported).

TEM image (Fig. 3a) presents some weak indication tentatively ascribable to nanoinhomogeneity, but hardly distinguishable from background fluctuations and contrast differences from variable sample thickness. Nevertheless, the electron diffraction pattern (Fig. 3g) registers a smooth increase of intensity just in the position of the (400) reflection of the spinel γ-Ga_2O_3 phase, consistent with the presence of a phase separation in the initial glass.

SANS experiments on nanostructuring

In Fig. 4 we report a summary of results from SANS experiments that give us valuable information on the evolution of the nanosized inhomogeneity in the investigated system and, importantly, of the real achievement of a nanostructured inhomogeneity in as-quenched glass. The results include the patterns collected on samples exposed to isothermal treatment at 670 °C for different time durations, and on samples subjected to isochronal treatments at different temperatures. Isochronal experiments comprise measurements on different samples each treated for 18 h at a temperature in the 610–670 °C range, and measurements on a single sample treated with successive 1 h heating processes at increasing temperature from 560 to 620 °C, in a step of 10 °C, after starting pre-treatment of 70 min at 550 °C and with a final treatment of 30 min at 630 °C. All curves show one maximum, indicating the occurrence of only one type of inhomogeneity. It is worth noting that a slightly pronounced maximum in the pattern of as-quenched glass reveals inhomogeneities even before any heat treatment.

The size $2R$ of these initial inhomogeneities, from the gyration radius R_g obtained from the slope of the Guinier plot ln(I) *vs.* q^2 after the maximum and using the approximation of hard spheres ($R^2 = 5R_g{}^2/3$), turns out to be 8 nm. The mean distance among scattering inhomogeneities, roughly estimated as $d = 2\pi/q_{max}$ from the position q_{max} of the maximum scattered intensity, is about 20 nm (Fig. 5 reports R_g and $q_{max}{}^{-1}$ values of all SANS experiments). After heat treatment, the main peak becomes sharper, and the scattered intensity increases but, interestingly, the whole scattering curve shifts toward higher wavevector values. As a consequence, after the first annealing step of as-quenched glass, q_{max} turns out to be larger and the slope of the curve, related to R_g, takes smaller values. The modified system is thus characterized by the smaller size of the

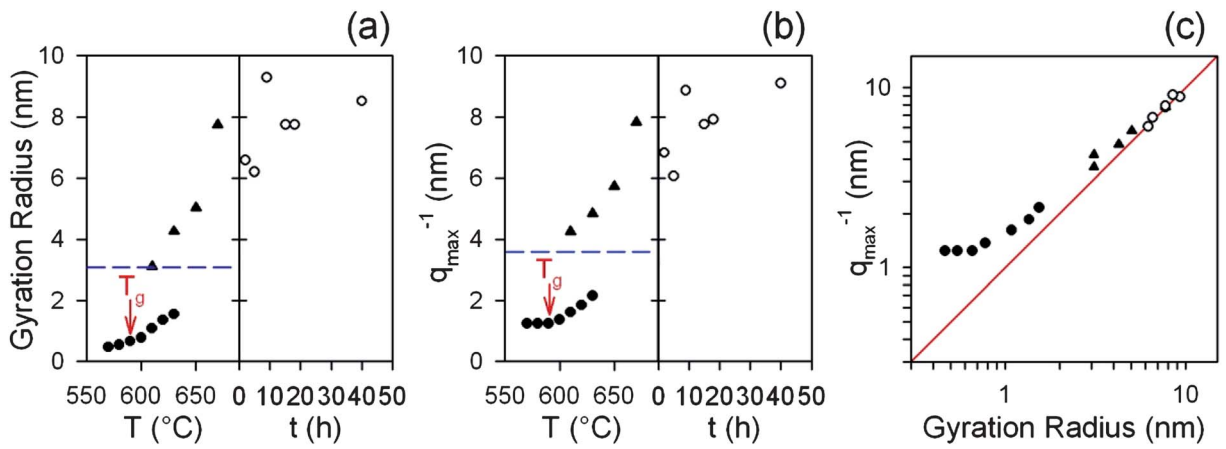

Fig. 5 (a) Gyration radius and (b) reciprocal of the wavevector at the maximum of SANS scattered intensity on a sample after successive annealing from 550 to 630 °C (filled circles), on different samples treated for 18 h at different temperatures ranging from 610 to 670 °C (triangles), and on samples subjected to isothermal annealing at 670 °C for different time durations (empty circles). (c) Relationship in the log–log plot between $q_{max}{}^{-1}$ and gyration radius (the straight line shows the linear slope). In (a) and (b), the glass transition temperature T_g is also indicated as well as R_g and $q_{max}{}^{-1}$ in as-quenched glass (dashed lines).

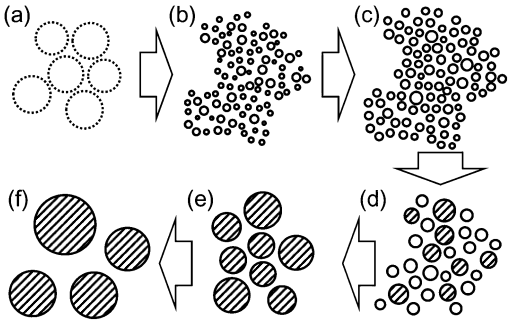

Fig. 6 Schematic view of the nanostructuring processes in Ga-modified germanosilicates as suggested by SANS experiments. (a) Initial amorphous inhomogeneity in as-quenched glass. (b) Thermally activated formation of small amorphous nanoparticles from secondary-like phase separation. (c) Nanoparticle growth at approaching glass transition temperature, with a constant average interparticle distance. (d) Onset of nanoparticle crystallization (dashed) and intensification of the ripening process with dissolution of smaller nanoparticles. (e) Full nanophase crystallization. (f) Nanocrystal growth driven by ripening or coalescence.

scattering objects accompanied by a smaller interparticle mean distance. Moreover, the higher scattered intensity indicates that the concentration and/or the density of the scattering nanoparticles (compared with the surrounding matrix) increases as well.

This result suggests that each initial nano-inhomogeneity does collapse in several reduced nanoparticles (see Fig. 6a and b). The collected SANS curves constitute clear-cut two-photogram evidence of glass–glass secondary separation – *i.e.* a phase segregation that starts from larger initial nanoinhomogeneity. In fact, nanostructuring processes in glass often proceed through amorphous phase separation near T_g with formation of particles of a few nm in diameter, as in MgO (or CaO or Li_2O or BaO)–Al_2O_3–SiO_2 TiO_2-containing glass,[26] but starting from a homogeneous amorphous matrix. In the present system, nanostructuring and subsequent nanocrystal formation start from initial Ga-oxide rich inhomogeneities through a secondary phase separation within these inhomogeneities. This process shows some similarities to typical mixed oxides in the immiscibility region.[29] However, in the present case, the initial inhomogeneity is quenched from the melt, probably starting from a liquid–liquid phase separation, as very recently observed by scanning transmission electron microscopy in high angle annular dark field mode.[27] From SANS data summarized in Fig. 5, we also note that after the first annealing step, further heat treatments lead to an increase of nanostructure sizes (from less than 2 to 20 nm), which is accompanied – except for the first steps of nanoparticle growth evidenced in *in situ* experiments – by a shift of the maximum of scattered intensity toward small wavevector values.

Looking at Fig. 5c, which collects q_{max}^{-1} and R_g values from all the performed SANS experiments, the growth of the nanophase proceeds by approaching a linear relationship between q_{max}^{-1} and R_g at prolonged treatment duration at temperature close to the exothermic crystallization peak. This suggests a decrease of interfacial area and the occurrence of Ostwald ripening processes, progressively more important at increasing temperature and treatment duration. This process works on the collapsed inhomogeneities, favoring large nanoparticles over the smallest ones (Fig. 6c and d), and reducing the interparticle distances as appears in the shift of the SANS correlation peak. Then the process proceeds through the coalescence of formed nanocrystals (Fig. 6d–f). The process is however limited by the increase of interparticle distance that follows the nanoparticle growth. As a matter of fact, the nanoparticle size does not increase sensibly above 20 nm. Analogously, TEM and XRD results show no relevant increase of size even after treatment prolonged for 90 h. Interestingly, SANS data indicate that the onset for this kind of mechanism is quite exactly concomitant with the glass transition, identified by DSC measurements at about 570 °C (Fig. 1). In fact, just above T_g, when the nanophase starts to crystallize, as indicated by XRD (Fig. 2), the increase of nanoparticle size is followed by the increase of interparticle distance, as one can argue by comparing the evolution of R_g and q_{max}^{-1} in Fig. 5a and b, respectively, and the clear-cut change in their relationship in Fig. 5c. A parallel increase of SANS intensity upon heat treatment and, in turn, of $\langle(\Delta\rho)^2\rangle$ is consistent with the progressive crystallization process, which leads to an increase of nanophase mean density.

Spectroscopic analysis of glass nanostructuring

The collapse of amorphous native inhomogeneities in small nanoparticles, and the following nanoparticle growth and crystallization, pose the problem of identifying the glass components that play pivotal roles and really drive these processes in the investigated glass. The spectroscopic analysis of the structural modifications at various steps of the

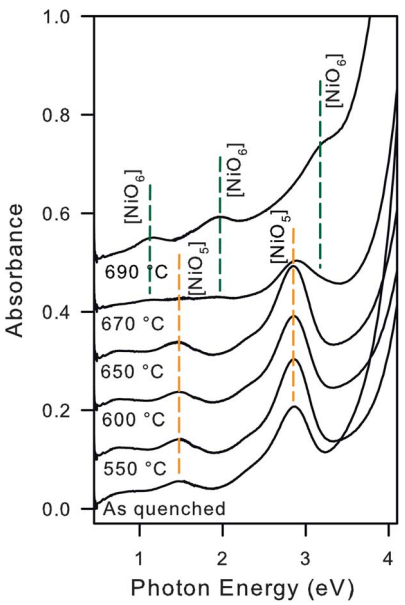

Fig. 7 Optical absorption spectra of 0.1 NiO-doped $7.5Li_2O$–$2.5Na_2O$–$20.0Ga_2O_3$–$35.0SiO_2$–$35.0GeO_2$ heat-treated at different temperatures. Orange and green lines indicate crystal field transitions of Ni^{2+} in five-fold glass-like and six-fold crystal-like coordination, respectively. Spectra are shifted by 0.1 absorbance unit from each other for clarity.

nanostructuring process gives indeed some first interesting indications.

The optical absorption spectrum of Ni^{2+} ions, introduced into the composition as doping species, gives us the opportunity to follow part of the structural changes from the amorphous system to the nanocrystallized materials. Fig. 7 reports optical absorption spectra collected on Ni-doped samples treated at different temperatures in a range comprising the glass transition temperature up to crystallization for 15 min. The spectral range is dominated by absorption bands caused by crystal field transitions of Ni^{2+} ions in two different types of environments – five-fold coordination, typical of Ni^{2+} in a glassy environment, and six-fold octahedral coordination as in crystalline gallium oxides.[16,21,24,30] Importantly, the Ni^{2+} spectrum starts to change at temperature lower than the crystallization temperature, clearly indicating a process of gradual ordering or, at least, the change of mean coordination of the structure. Close to the crystallization (sample treated at 670 °C), the spectrum gives indication of an intermediate situation, with the coexistence of five-fold glassy-like and six-fold crystal-like coordinations around Ni ions. Taking into account that Ni^{2+} substitutes for Ga^{3+} in the final nanocrystals,[24] we can argue that gallium likely follows a similar gradual change of coordination and fills octahedral sites well before crystallization completion.

Fig. 8 indeed supports the occurrence of structural changes. IR spectra show the relevant changes at about 650 cm^{-1}, where the intensity in the region of tetrahedral vibrational modes of Ga oxide phases[31,32] increases with time and temperature of the thermal treatment. This latter result is only apparently in contrast with Ga-oxide crystallization, which is expected to decrease the number of low-coordinated Ga sites in favor of octahedral Ga sites that in turn are incompatible with the amorphous network of the glass matrix in which Ga is substituted for tetrahedral Si or Ge sites.

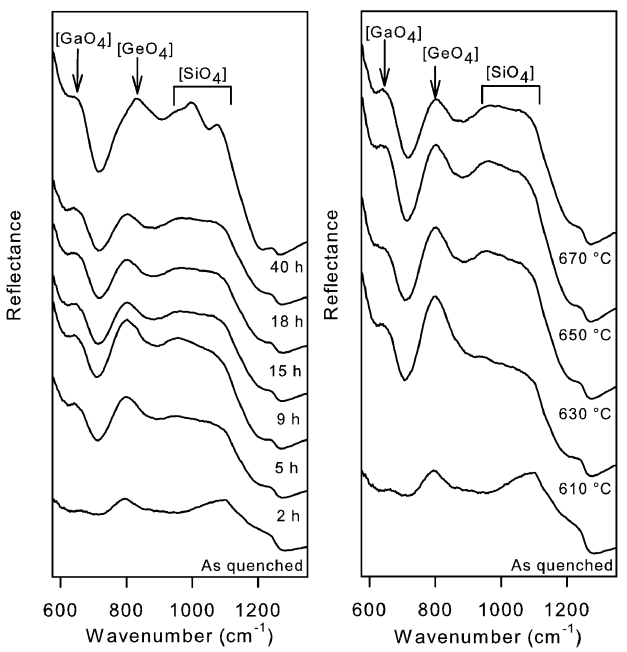

Fig. 8 (left) IR reflectance spectra of samples treated for different times at 670 °C and (right) for 18 h at different temperatures.

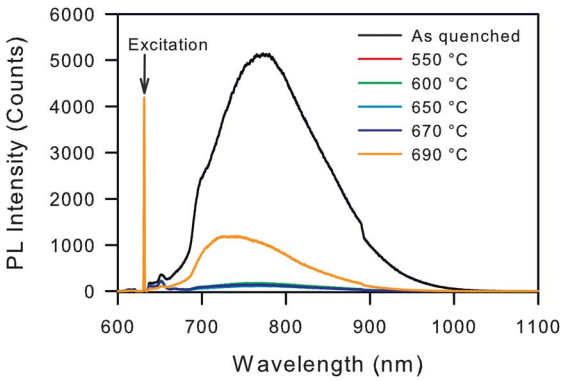

Fig. 9 Photoluminescence spectra excited at 633 nm in the as-quenched sample and in samples heat-treated at different temperatures.

In fact, in glass, Ga sites are expected to be in defective tetrahedral sites, connected with non-bridging oxygen (NBO) and charge compensating alkali ions. Instead, the progressive ordering of the separated Ga oxide phase provides an ideal tetrahedral site, not perturbed by charge compensators. Therefore, from different perspectives, optical absorption and IR spectroscopies register the occurrence of a relevant change of cation coordination number preliminary to the stabilization of six-fold octahedral sites and regular tetrahedral sites of the fully crystallized nanoparticles in the γ-Ga_2O_3 phase. Importantly, this indication suggests a relevant rearrangement in the glass matrix. Photoluminescence spectra excited at 633 nm indeed confirm this view. As shown in Fig. 9, the typical red-light emission of NBO sites in oxides[33–37] is much higher in as-quenched glass than in treated samples, except when the treatment temperature approaches the crystallization point. The high NBO PL in as-quenched glass suggests a structure with a large fraction of Ga ions in sites coordinated with NBOs.

The initial strong decrease suggests a thermally induced readjustment of the glass network driven by Ga segregation in collapsed small nanoparticles within the pre-existent inhomogeneities, as suggested by SANS data, with the decrease of NBOs. Finally, NBOs increase again approaching the crystallization point, probably when the interface of the separated phase ceases to be blurred and adjusts the structural mismatch through coordination defects.

Conclusions

The complementary indications obtained from SANS, TEM, and XRD and from the spectroscopic monitoring of glass structural modifications give for the first time some insights into the structural peculiarity induced by Ga addition to the network of alkali germanosilicates. In particular, SANS data give the clear-cut evidence of phase separation in as-quenched glass at the nanometer scale. This kind of nano-inhomogeneities act as nucleation sites for thermally activated segregation of a Ga-oxide phase, which can finally be brought to crystallization with

formation of γ-Ga_2O_3 nanoparticles embedded in an amorphous germanosilicate matrix. The knowledge gained on the details of the nanostructuring process gives the possibility to better tailor the nanostructure of Ga-containing glass for specific applications.

Acknowledgements

This work is supported by the Ministry of Education and Science of Russia under Grant no. 11.G34.31.0027, PICS France-Russia no. 5584 (RFBR no. 10-03-91056) and Russian Foundation for Basic Research (Grant no. 12-03-31711). We gratefully acknowledge Lionel Porcar for his expertise on the ILL-D11 experiment.

Notes and references

1 G. N. Greaves, M. C. Wilding, S. Fearn, D. Langstaff, F. Kargl, S. Cox, Q. Vu Van, O. Majérus, C. J. Benmore, R. Weber, C. M. Martin and L. Hennet, *Science*, 2008, **322**, 566.
2 L. L. Beecroft and C. K. Ober, *Chem. Mater.*, 1997, **9**, 1302.
3 B. N. Samson, L. R. Pinckney, J. Wang, G. H. Beall and N. F. Borrelli, *Opt. Lett.*, 2002, **27**, 1309.
4 S. Brovelli, N. Chiodini, A. Lauria and A. Paleari, *J. Nanopart. Res.*, 2008, **10**, 737.
5 J. del-Castillo, V. D. Rodríguez, A. C. Yanes and J. Méndez-Ramos, *J. Nanopart. Res.*, 2008, **10**, 499.
6 A. C. Yanes, J. del-Castillo, J. Méndez-Ramos and V. D. Rodríguez, *J. Nanopart. Res.*, 2011, **13**, 7295.
7 S. Brovelli, N. Chiodini, R. Lorenzi, A. Lauria, M. Romagnoli and A. Paleari, *Nat. Commun.*, 2012, **3**, 690.
8 I. Yamaguchi, K. Tanaka, K. Hirao and N. Soga, *J. Mater. Sci.*, 1996, **31**, 3541.
9 T. Suzuki, G. S. Murugan and Y. Ohishi, *Appl. Phys. Lett.*, 2005, **86**, 131903.
10 S. Zhou, G. Feng, B. Wu, N. Jiang, S. Xu and J. Qiu, *J. Phys. Chem. C*, 2007, **111**, 7335.
11 S. Zhou, H. Dong, G. Feng, B. Wu, H. Zeng and J. Qiu, *Opt. Express*, 2007, **15**, 5477.
12 S. Xu, D. Deng, R. Bao, H. Ju, S. Zhao, H. Wang and B. Wang, *J. Opt. Soc. Am. B*, 2008, **25**, 1548.
13 S. Zhou, N. Jiang, H. Dong, H. Zeng, J. Hao and J. Qiu, *Nanotechnology*, 2008, **19**, 015702.
14 T. Suzuki, Y. Arai and Y. Ohishi, *J. Lumin.*, 2008, **128**, 603.
15 Y. Zhuang, Y. Teng, J. Luo, B. Zhu, Y. Chi, E. Wu, H. Zeng and J. Qiu, *Appl. Phys. Lett.*, 2009, **95**, 111913.
16 S. Zhou, N. Jiang, B. Wu, J. Hao and J. Qiu, *Adv. Funct. Mater.*, 2009, **19**, 2081.
17 T. Suzuki, Y. Arai and Y. Ohishi, *J. Non-Cryst. Solids*, 2007, **353**, 36.
18 Y. Zhuang, M. Guan, J. Xie, Y. Teng, J. Zhou, S. Zhou, J. Ruan and J. Qiu, *J. Phys. D: Appl. Phys.*, 2010, **43**, 095401.
19 N. V. Golubev, V. I. Savinkov, E. S. Ignat'eva, S. V. Lotarev, P. D. Sarkisov, V. N. Sigaev, L. I. Bulatov, V. M. Mashinskii, V. G. Plotnichenko and E. M. Dianov, *Glass Phys. Chem.*, 2010, **36**, 657.
20 S. Zhou, N. Jiang, K. Miura, S. Tanabe, M. Shimizu, M. Sakakura, Y. Shimotsuma, M. Nishi, J. Qiu and K. Hirao, *J. Am. Chem. Soc.*, 2010, **132**, 17945.
21 D. Deng, H. Ma, S. Xu, Q. Wang, L. Huang, S. Zhao, H. Wang and C. Li, *J. Non-Cryst. Solids*, 2011, **357**, 1426.
22 S. Zhou, J. Hao and J. Qiu, *J. Am. Ceram. Soc.*, 2011, **94**, 2902.
23 K. Zhang, S. Zhou, Y. Zhuang, R. Yang and J. Qiu, *Opt. Express*, 2012, **20**, 8675.
24 V. N. Sigaev, V. N. Golubev, E. S. Ignat'eva, V. I. Savinkov, M. Campione, R. Lorenzi, F. Meinardi and A. Paleari, *Nanotechnology*, 2012, **23**, 015708.
25 P. A. Tick, N. F. Borrelli and I. M. Reaney, *Opt. Mater.*, 2000, **15**, 81.
26 A. A. Loshmanov, V. N. Sigaev, R. Y. Khodakovskaya, N. M. Pavlushkin and I. I. Yamzin, *J. Appl. Crystallogr.*, 1974, **7**, 207.
27 O. Dargaud, L. Cormier, N. Menguy and G. Patriarche, *J. Non-Cryst. Solids*, 2012, **358**, 1257.
28 A. B. Seddon, V. K. Tikhomirov, H. Rowe and D. Furniss, *J. Mater. Sci.: Mater. Electron.*, 2007, **18**, S145.
29 R. R. Shaw and J. F. Breedis, *J. Am. Ceram. Soc.*, 1972, **55**, 422.
30 L. Galoisy and G. Calas, *Geochim. Cosmochim. Acta*, 1993, **57**, 3613.
31 J. A. Ruller and J. M. Jewell, *J. Non-Cryst. Solids*, 1994, **175**, 91.
32 H. Fan, G. Wang and L. Hu, *Solid State Sci.*, 2009, **11**, 2065.
33 P. D. Dragic, C. G. Carlson and A. Croteau, *Opt. Express*, 2008, **16**, 4688.
34 L. El Mir, A. Amlouk, C. Barthou and S. Alaya, *Mat. Sci. Eng., C - Mater*, 2008, **28**, 771.
35 L. Skuja, *J. Non-Cryst. Solids*, 1994, **179**, 51.
36 T. Suzuki, L. Skuja, K. Kajihara, M. Hirano, T. Kamiya and H. Hosono, *Phys. Rev. Lett.*, 2003, **90**, 186404.
37 V. M. Mashinsky, N. M. Karatun, V. A. Bogatyrev, V. N. Sigaev, N. V. Golubev, E. S. Ignat'eva, R. Lorenzi, M. C. Mozzati, A. Paleari and E. M. Dianov, *Microsc. Microanal.*, 2012, **18**, 259.

